



Title	Reduction of friction of steel covered with oxide scale in hot forging
Author(s)	Matsumoto, Ryo; Osumi, Yuta; Utsunomiya, Hiroshi
Citation	Journal of Materials Processing Technology. 2014, 214(3), p. 651-659
Version Type	AM
URL	<a href="https://hdl.handle.net/11094/93999">https://hdl.handle.net/11094/93999</a>
rights	© 2014. This manuscript version is made available under the CC-BY-NC-ND 4.0 license <a href="https://creativecommons.org/licenses/by-nc-nd/4.0/">https://creativecommons.org/licenses/by-nc-nd/4.0/</a>
Note	

*The University of Osaka Institutional Knowledge Archive : OUKA*

<https://ir.library.osaka-u.ac.jp/>

The University of Osaka

Title:

## Reduction of Friction of Steel Covered with Oxide Scale in Hot Forging

Authors:

Ryo Matsumoto<sup>1,\*</sup>, Yuta Osumi<sup>2</sup> and Hiroshi Utsunomiya<sup>1</sup>

\* Corresponding author (R. Matsumoto, E-mail: ryo@mat.eng.osaka-u.ac.jp, Tel: +81-6-6879-7500, Fax: +81-6-6879-7500)

Affiliation:

<sup>1</sup> Division of Materials and Manufacturing Science, Graduate School of Engineering, Osaka University, 2-1 Yamadaoka, Suita 565-0871, Japan

<sup>2</sup> Division of Mechanical Engineering, Graduate School of Engineering Science, Osaka University, 1-3 Machikaneyama, Toyonaka 560-8531, Japan

### Abstract

The hot ring compression test of chrome steel covered with an oxide scale film is carried out to examine the effects of the oxide scale film on the hot forging characteristics through experiment and finite element analysis. The nominal coefficient of shear friction of the scale is estimated from the plastic deformation behavior of the chrome steel covered with oxide scale film. The estimated coefficient of shear friction of the oxide scale is found to be lower than that of the chrome steel. The plastic deformations and temperature changes of the chrome steel workpiece and the oxide scale layer are calculated using finite element analysis method to investigate the mechanism underlying the reduction in the friction during the hot forging of chrome steel covered with an oxide scale film. Low friction and thermal conductivity values of the oxide scale lead to low forging load in the hot forging of chrome steel covered with an oxide scale film.

Keywords: Oxide scale; Steel; Friction; Forging

## 1. Introduction

An oxide scale film is generated on steel surfaces at elevated temperatures in the presence of air. Because the scale is located at the interface between tool and steel workpiece during hot working processes, it crucially influences the hot working characteristics. It is known that the friction and heat transfer characteristics in the hot working processes are affected by the presence of scale. Utsunomiya et al. (2009) have recently developed a technique for preserving the scale using glass powder during hot rolling, and then Hara et al. (2011) have investigated the deformation behavior of the scale during hot rolling processes. Munther and Lenard (1999) have suggested that scale reduces friction during hot rolling processes. Okada (2003) has examined the deformation behavior and crack initiation in a scale in hot rolling processes. Torres and Colás (2000) have examined the heat conduction properties of a scale, and Guerrero et al. (1999) have proposed the heat transfer model with consideration of oxide layer in hot rolling. Krzyzanowski and Beynon (2002) have measured oxide properties for numerical analysis under hot rolling condition. Garza-Montes-de-Oca and Rainforth (2009) have investigated the influence of oxidation of the roll surface on the wear in hot rolling. Thus, the hot rolling characteristics of scale have been mainly investigated. On the other hand, Suárez et al. (2011) have investigated the deformation behavior of the oxide layer of ultra-low carbon steel in plane strain compression. Hidaka et al. (2002) have measured the mechanical properties, deformation and fracture behaviors of iron oxides at elevated temperatures to understand the properties of a scale.

Most of the scale generated on steel surfaces is removed by a descaling process immediately prior to hot working (i.e., hot rolling), and the remaining thin secondary scale tends to deform with the steel. The volume fraction of the scale relative to the steel workpiece is generally low because workpieces with large volume are usually used in primary hot working processes. On the other hand, the volume fraction of the scale relative to a steel

workpiece in secondary hot forging processes of steel, such as the hot forging of automotive parts, is comparatively high because these processes are typically applied to workpieces with small volume. The influence of the scale on the hot forging characteristics is crucial in the context of secondary hot forging processes.

Recent manufacturing technologies have desired to produce the hot forging of products with a high dimensional accuracy or complicated shape. To realize the demands for such products, Douglas and Kuhlmann (2000) have developed precision flashless hot forging and near net-shape hot forging processes. Doege and Bohnsack (2000), and Behrens et al. (2007) have proposed novel tool concepts for achieving precision hot forging. Gladkov (2006) has developed a hot die forging press with a closed gap adjustment mechanism for the production of precision forged-products. Nakasaki et al. (2006) have examined hot forging of hub bearing parts without burrs using CAE analysis. One of other solutions for realizing precision hot forging processes relies on controlling the deformation behavior of the scale, which is located at the interface between the tool and the workpiece.

In this study, the scale grown on a chrome steel workpiece surface is focused. The scale generated on the chrome steel workpiece surface is examined with respect to its effects on the hot forging characteristics of the workpiece using a hot ring compression test. The nominal coefficient of shear friction of the scale is estimated from the plastic deformation behavior of the chrome steel workpiece covered with the oxide scale film. The mechanism underlying the reduction in friction with the scale during hot forging is discussed with experimental results and a finite element analysis.

## **2. Experimental set-up**

### **2.1. Oxidation test**

The oxidation properties of chrome steel JIS SCr420 (Fe-0.2mass% C-1.0mass% Cr,

Table 1) were investigated. The chrome steel workpiece was heated and oxidized at  $T_o = 1073\text{--}1423$  K in an electric furnace under an air atmosphere. The oxidized workpiece was taken out from the furnace after oxidation for oxidation duration  $t_o = 0\text{--}1.8 \times 10^4$  seconds. The surface of the oxidized workpiece was then immediately coated with a PbO-B<sub>2</sub>O<sub>3</sub>-based glass powder. The oxide scale generated during oxidation in the furnace was preserved by applying a surface coating comprising the PbO-B<sub>2</sub>O<sub>3</sub>-based glass without using a special apparatus (Utsunomiya et al., 2009).

Table 1 Chemical compositions of chrome steel workpiece used in this study. (mass%)

C	Si	Mn	P	S	Cr	Fe
0.20	0.25	0.60	<0.03	<0.03	1.05	Bal.

## 2.2. Ring compression test

The friction properties of the chrome steel covered with an oxide scale film during hot forging process were measured using the ring compression test. In the test, a ring-shaped workpiece was compressed between flat parallel tools and the friction was estimated by varying the inner diameter of the workpiece (Male and Cockcroft, 1964-65). Since this method does not necessitate a load measurement, it is frequently used to estimate friction during forging when the workpiece does not undergo a large surface expansion. The initial ring-shaped workpiece having a ratio of outer diameter ( $D_0$ ): inner diameter ( $d_0$ ): height ( $h_0$ ) = 6: 3: 2 is usually employed.

In this study, a chrome steel workpiece with an initial shape of  $D_0 = 18.0$  mm,  $d_0 = 9.0$  mm and  $h_0 = 6.0$  mm was compressed between tools with tungsten carbide (WC-20mass%Co). The surface roughness values of the workpiece and the tools were  $Ra = 0.30\text{--}0.50$   $\mu\text{m}$  and  $0.02\text{--}0.04$   $\mu\text{m}$ , respectively. The ring-shaped workpiece was heated and

oxidized in an electric furnace at  $T_0 = 1273$  K under an air atmosphere, and the oxide scale thickness was controlled according to the oxide scale thickness-oxidation duration relationship (see Fig. 5) prior to applying the ring compression test. The oxidized workpiece having an oxide scale film with a thickness of  $h_{s0} = 0\text{--}300$   $\mu\text{m}$  was compressed between the tools under dry (unlubricated) condition at an initial workpiece temperature of 1273 K. The test was conducted using a 450 kN servo press (Komatsu Industrial Corp., H1F45). Because the servo press was driven by an AC servomotor through a mechanical link (0–70 spm), the press ram speed and motion could be controlled as shown in Fig. 1. The ring-shaped workpiece covered with an oxide scale film was forged with an average strain rate ( $\dot{\epsilon}_{\text{avg}}$ ) of  $2.8$   $\text{s}^{-1}$  with a maximum reduction in height ( $\Delta h/h_0$ ) of 60%. The test was conducted three times under each condition. To prevent secondary oxidation of the upper and lower surfaces of the forged workpiece, the upper tool was held at the bottom dead center of the press for 60 seconds immediately after forging and the forged workpiece was sandwiched between the tools without allowing the upper and lower surfaces of the forged workpiece to contact air. The forged workpiece was cooled to a temperature below 323 K during the sandwiching of the forged workpiece between tools, and the workpiece was not extensively oxidized. The ram motion control of the press after forging permitted the plastic deformation of the oxide scale to be examined during hot forging. The minimum inner diameter of the workpiece at the center of the workpiece (along the vertical direction) was measured using a microscope to estimate the coefficient of shear friction of the workpiece.

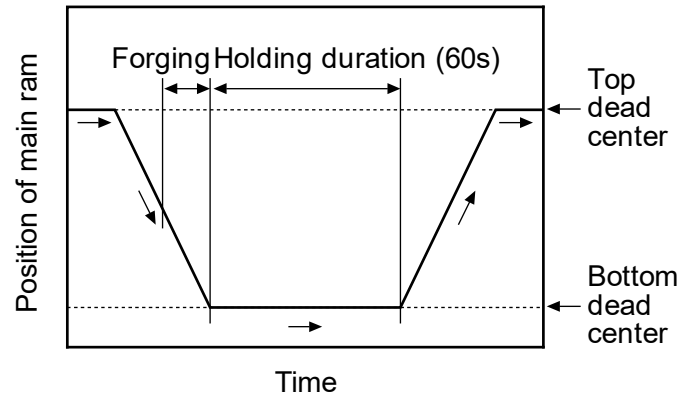


Fig. 1 Illustration of press ram motion for the ring compression test on a servo press.

### 3. Finite element analysis conditions

The relationship between the friction and the plastic deformation of the chrome steel covered with an oxide scale formed at elevated temperatures in a ring compression test was examined using a finite element simulation code. A commercial three-dimensional finite element code DEFORM-3D ver.10.2 SP1 (Scientific Forming Technologies Corporation) was employed. In the simulation, a rigid-plastic finite element method for plastic deformation and a heat conduction finite element method for temperature change were employed to calculate the stress, strain states, and temperature distributions of the workpiece and the oxide scale at each calculation step during the ring compression. The tools were treated as rigid bodies. The simulation model is illustrated in Fig. 2. A 30 degrees section of the ring-shaped workpiece was analyzed with consideration for the symmetry of the ring compression geometry. A scale with an initial thickness of  $h_{s0} = 0\text{--}300\ \mu\text{m}$  was allocated onto the upper and lower surfaces of the workpiece, whereas the scale was not allocated onto the side surfaces of the workpiece. A tetrahedral mesh was employed to model the workpiece and the scale. The average volume of the initial mesh was about  $3.0 \times 10^{-3}\ \text{mm}^3$ . The elements were automatically re-meshed at each calculation step, depending on the plastic deformation of each element.

Table 2 shows the computational conditions used to simulate the ring compression

test. The initial geometries and temperatures of the chrome steel workpiece, scale layer, and tools used for the simulation were identical to the experimental values. The cross-section of the scale layer generated on surface of the chrome steel workpiece is shown in Fig. 3. The scale layer was composed of four phases of FeO, Fe<sub>3</sub>O<sub>4</sub>, Fe<sub>2</sub>O<sub>3</sub> and FeCr<sub>2</sub>O<sub>4</sub>, however, the scale layer was simply assumed to be FeO single-phase in the simulation because the primary composition of the scale was FeO. The heat transfer coefficients at the tool–workpiece contact interfaces and at the free surfaces were determined experimentally using heating and cooling tests on the workpiece. In the heating and cooling tests, the temperature change of the workpiece surface with contacting the tool or air was measured by thermocouple. The measured temperature changes were compared with the finite element analysis results under various heat transfer coefficients conditions. The heat transfer coefficients at the tool–scale and the scale–workpiece contact interfaces were assumed to be equal to the heat transfer coefficient at the tool–workpiece contact interfaces. The frictional coefficients were assumed to obey the shear friction law (Schey, 1983). The coefficients of shear friction at the tool–workpiece contact interfaces and the tool–scale contact interfaces were given as  $m_{t-w} = 0-1.0$  and  $m_{t-s} = 0-1.0$ , respectively. The coefficient of shear friction at the scale–workpiece contact interfaces was assumed to be  $m_{s-w} = 1.0$  (no sliding). Literature values were used to define the density (Krzyzanowski et al., 2010), specific heat (Krzyzanowski et al., 2010; Touloukian and Buyco, 1970), and thermal conductivity (Touloukian et al., 1970; Akiyama et al., 1991) of the chrome steel workpiece and the scale (FeO) at various temperatures.

The flow stress curves of the chrome steel workpiece were measured using upsetting test at  $\dot{\epsilon}_{\text{avg}} = 1.3$  and  $3.4 \text{ s}^{-1}$  at various temperatures. The measured flow stress curves included the influence of the workpiece temperature change during the upsetting because heat was generated by the plastic deformation and transferred by heat transfer between the workpiece surface and the tools. The influence of the temperature change during the upsetting

test was removed from the measured flow stress curves by applying a calculation method proposed by Kada et al., (1998). In this method, the isothermal flow stress was calculated by combining the experimental results from the upsetting test with a finite element analysis. The flow stress curves of the chrome steel workpiece obtained at various temperatures are shown in Fig. 4. The strain rate sensitivity exponent  $m$ -value of the chrome steel workpiece was determined to be 0.138 based on the data shown in Fig. 4. On the other hand, the literature values (Torres and Colas, 2000; Graf and Kawalla, 2011; Graf and Kawalla, 2012) were derived from the flow stress curves of the scale at elevated temperatures. The constitutive relation used in the simulation was a multilinear isotropic hardening determined from the stress–strain curves of the chrome steel workpiece and the scale. The temperature dependences of the flow stress curves were obtained by linear interpolation. The occurrences of crack of the chrome steel workpiece and the scale were not considered in this analysis.

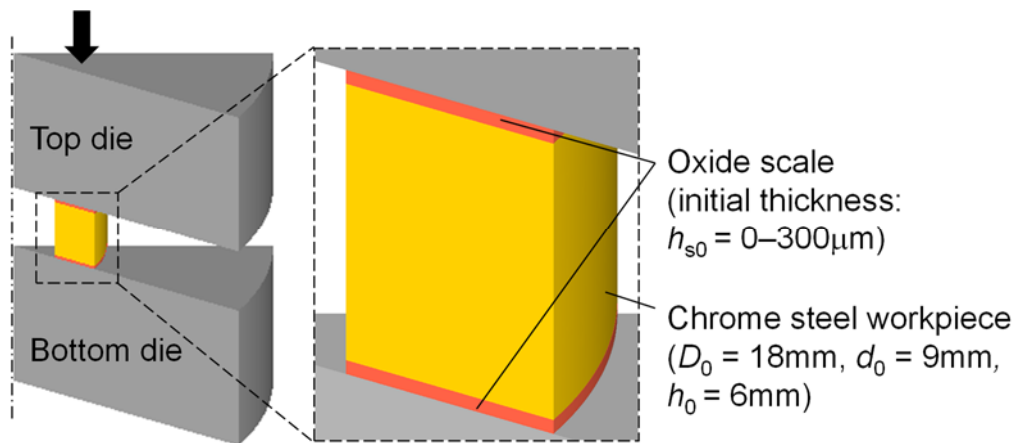
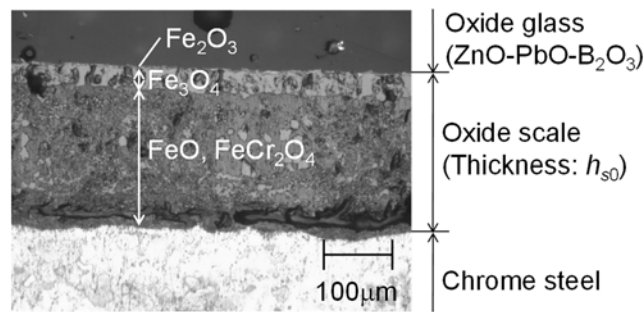


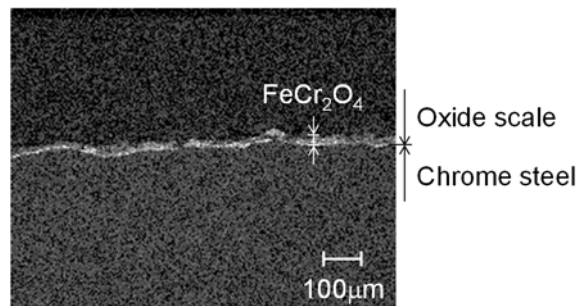
Fig. 2 Finite element analysis model for the ring compression test of chrome steel workpiece having oxide scale layers on top and bottom surfaces.

Table 2 Computational conditions used for finite element simulation of the ring compression test.

Initial chrome steel workpiece temperature /K		1273
Initial oxide scale temperature /K		1273
Tool temperature /K		293
Air temperature /K		293
Heat transfer coefficient /W/(m <sup>2</sup> ·K)	Tool–workpiece contact	30000
	Tool–oxide scale contact	30000
	Oxide scale–workpiece contact	30000
	Free surface	150
Coefficient of shear friction	Tool–workpiece contact $m_{t-w}$	0–1.0
	Tool–oxide scale contact $m_{t-s}$	0–1.0
	Oxide scale–workpiece contact $m_{s-w}$	1.0 (no sliding)



(a) Photograph by optical microscope.



(b) Element map image of chrome by energy dispersive x-ray spectrometry (EDX).

Fig. 3 Cross-section of oxide scale layer generated on surface of chrome steel workpiece (Oxidation temperature  $T_o = 1273$  K).

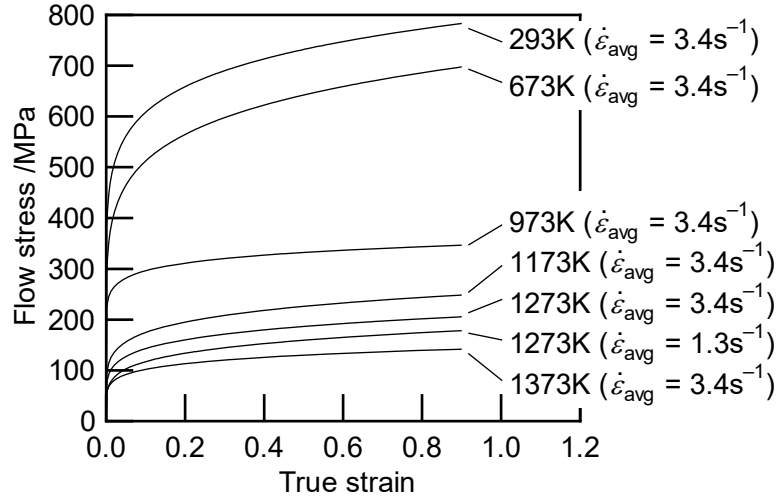


Fig. 4 Isothermal flow stress curves of the chrome steel workpiece at various temperatures

( $\dot{\epsilon}_{\text{avg}}$  : average strain rate).

## 4. Experimental results

### 4.1 Oxidation test

During the oxidation test, the chrome steel workpiece oxidized slightly at  $T_o < 1073$  K, and oxidation proceeded more extensively at  $T_o > 1423$  K. For these reasons, the thickness of the scale could not be measured accurately within these oxidation temperature ranges. The relationship between the scale thickness ( $h_s$ ) on the chrome steel surface and the oxidation duration ( $t_o$ ) at  $T_o = 1173$ – $1373$  K is shown in Fig. 5. The thickness of the scale increased with increasing oxidation temperature and duration. The scale thickness was not zero at  $t_o = 0$  s because about five seconds was required to coat the workpiece with a glass powder after the oxidized workpiece had been taken out from the furnace and secondary oxidation of the workpiece was inevitable. Here, the scale thickness increase ( $\Delta h_s$ ) could be described according to the following equation:

$$\Delta h_s = K t_o^{1/2} \quad (1)$$

where  $K$  is the oxidation velocity coefficient. Based on the data shown in Fig. 5, the

relationship between the scale thickness increase on the chrome steel surface and the oxidation duration could be plotted, as shown in Fig. 6. The oxidation velocity coefficients at  $T_o = 1173, 1273,$  and  $1373$  K were estimated from Fig. 6 to be  $K = 0.89, 4.84,$  and  $7.88,$  respectively. The Arrhenius equation (Callister, 2006) is described as a follows:

$$K = A \exp(Q/RT_o) \quad (2)$$

where  $A$  is the frequency factor,  $Q$  is the activation energy and  $R$  is the gas constant. The activation energy was estimated to be  $Q = 81.7$  kJ/mol based on the relationship between oxidation velocity coefficient and the oxidation temperature. The activation energy associated with oxidizing carbon steel is in the range of  $73.1$ – $138.0$  kJ/mol according to the literature (Munther and Lenard, 1999; Abuluwefa et al., 1997; Stanley et al., 1951). Thus, the estimated activation energy in this study was in reasonable agreement, and the thickness of the scale coated with glass was adequately measured.

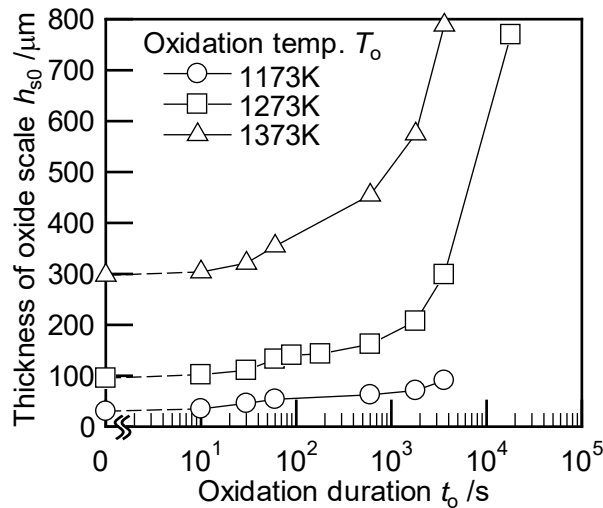


Fig. 5 Relationship between oxide scale thickness on the chrome steel surface and oxidation duration at elevated temperatures.

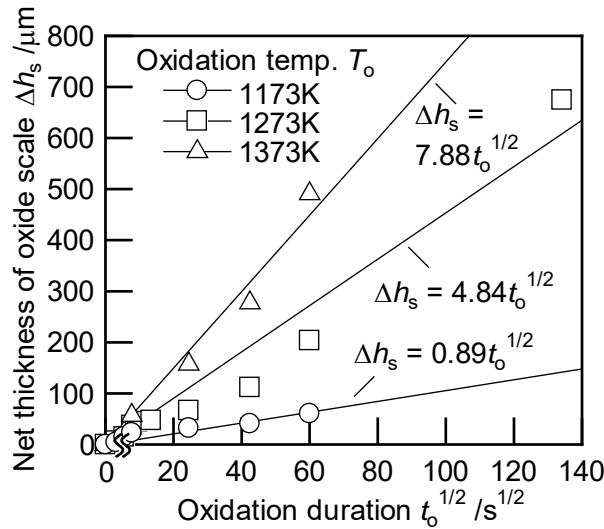


Fig. 6 Relationship between net oxide scale thickness on the chrome steel surface and oxidation duration at elevated temperatures.

#### 4.2 Friction in the ring compression test

Figure 7 shows the calibration curves for the relationship between the coefficient of shear friction at the tool–workpiece contact ( $m_{t-w}$ ) and the change in the inner diameter ( $d/d_0$ ) of the workpiece without scale film ( $h_{s0} = 0 \mu m$ ) in the ring compression test. The plastic deformation of the workpiece was calculated under various coefficients of shear friction for the tool–workpiece contact using finite element analysis methods. The inner diameter of the workpiece was varied with the coefficient of shear friction, and the change was particularly sensitive to the friction at  $m_{t-w} < 0.5$ . The marks plotted in Fig. 7 show the experimentally measured relationship between the change in the inner diameter ( $d/d_0$ ) and the reduction in height ( $\Delta h/h_0$ ) after compressing the ring-shaped workpieces. The scale thickness on the workpiece surface prior to the compression step was controlled according to the oxidation duration in the furnace at  $T_o = 1273$  K. The nominal coefficient of shear friction at the tool–workpiece contact ( $m_{t-w}$ ) was estimated based on a comparison between the experimental results (plotted marks) and the calibration curves shown in Fig. 7.

Figure 8 shows the estimated nominal coefficient of shear friction at the tool–workpiece contact ( $m_{nom}$ ) during compression of the workpiece covered with a scale film. A high friction value ( $m_{nom} > 0.6$ ) was obtained for the workpiece covered with a thin scale film ( $h_{s0} = 6 \mu\text{m}$ ). The nominal coefficient of shear friction decreased as the scale film thickness increased, and the nominal coefficient of shear friction for the workpiece having a scale film with  $h_{s0} = 300 \mu\text{m}$  was estimated to be  $m_{nom} =$  about 0.3. The forging load of the workpiece covered with a scale film during the ring compression was shown in Fig. 9. The forging load of the workpiece having a scale film with  $h_{s0} > 95 \mu\text{m}$  was approximately 20% lower than the value for a workpiece having a scale film with  $h_{s0} = 6 \mu\text{m}$ . The scale was found to reduce the friction and forging load during hot forging processes.

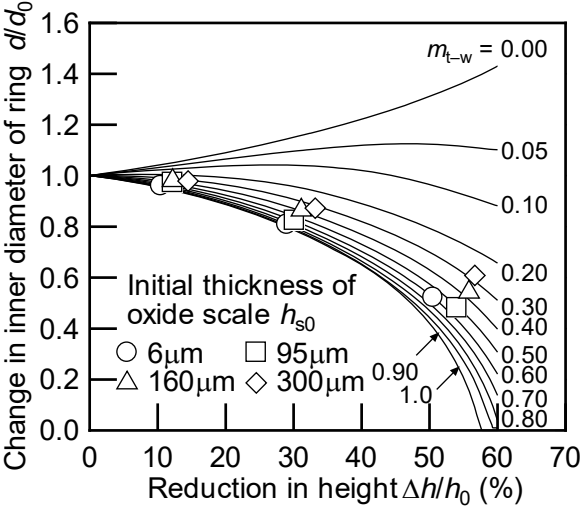


Fig. 7 Change in inner diameter of ring-shaped workpiece under various coefficients of shear friction at tool–workpiece contact ( $m_{t-w}$ ) (lines: finite element analysis), and experimental results of plastic deformation of workpiece during the ring compression test (plotted marks).

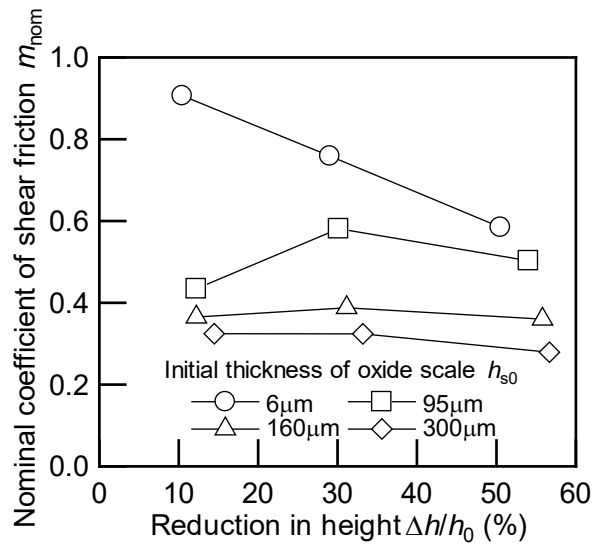


Fig. 8 Estimated nominal coefficient of shear friction for chrome steel covered with oxide scale film during the ring compression test.

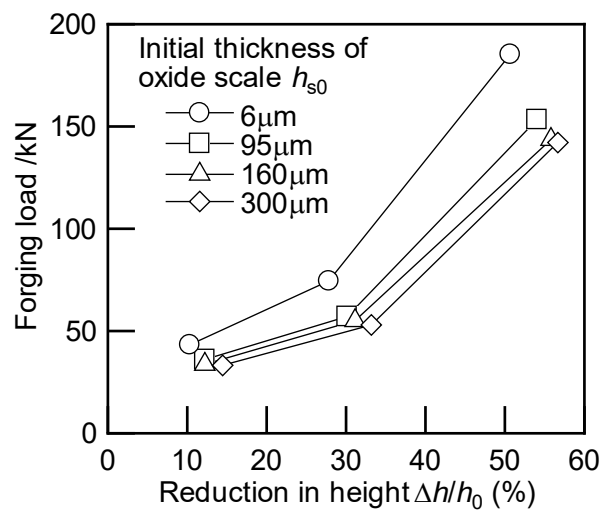


Fig. 9 Forging load on a chrome steel workpiece covered with oxide scale film in the ring compression test.

#### 4.3 Deformation behavior of the oxide scale in the ring compression test

Photographs showing cross-sectional images of the scale–workpiece interface around the tool contact surface after the ring compression test are displayed in Fig. 10. The scale was confined between the tool and the workpiece, and extended to be radius direction with the

workpiece. The workpiece then directly contacted with the tool near the inner and outer peripheries, as shown in Figs. 10(a3) and (b3). Figure 11 shows scanning electron microscopy (SEM) photographs of the cross-sections of the scale–workpiece interface after conducting the ring compression test. Cracks were not observed in the workpiece, whereas some cracks in the scale were appeared oriented along a direction parallel to the compression direction. These cracks appeared from the early stages of forging because the scale was cooled rapidly by contacting with the tool of room temperature during forging and sandwiching between the tools just after forging. The ductility of FeO (the primary composition of the scale) is lower than that of chrome steel (Hidaka et al., 2002), however, the primary cause of cracking in the scale has not yet been identified. Either the rapid cooling or the low ductility of the scale could be responsible for crack initiation.

The measured thicknesses of the scales on the compressed surfaces are shown in Fig. 12. The scales with  $h_{s0} = 95$  and  $160 \mu\text{m}$  became thinner by about  $10 \mu\text{m}$  when the height of the workpiece was reduced by 10%. The scale with  $h_{s0} = 300 \mu\text{m}$  displayed a larger decrease in the ratio of the scale thickness in  $\Delta h/h_0 = 30\text{--}50\%$ , as compared to the scales with  $h_{s0} = 95$  and  $160 \mu\text{m}$  in  $\Delta h/h_0 = 10\text{--}30\%$ . Figures 10(b) and 12 clearly show that the scale was confined between the tool and workpiece during the early stage of forging. The scale was subsequently extended along the radial direction of the workpiece after the middle stage of the forging process.

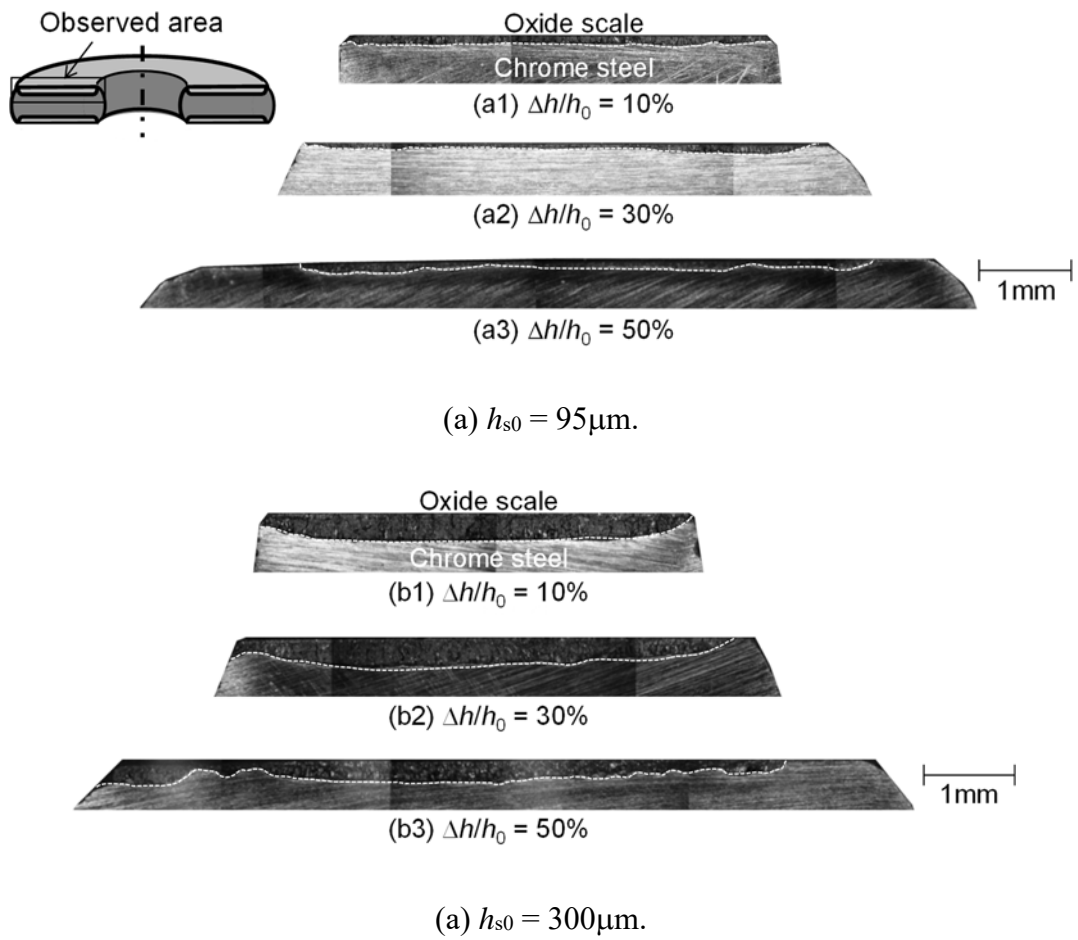


Fig. 10 Photographs of cross-section of oxide scale–chrome steel workpiece interface after the ring compression test.

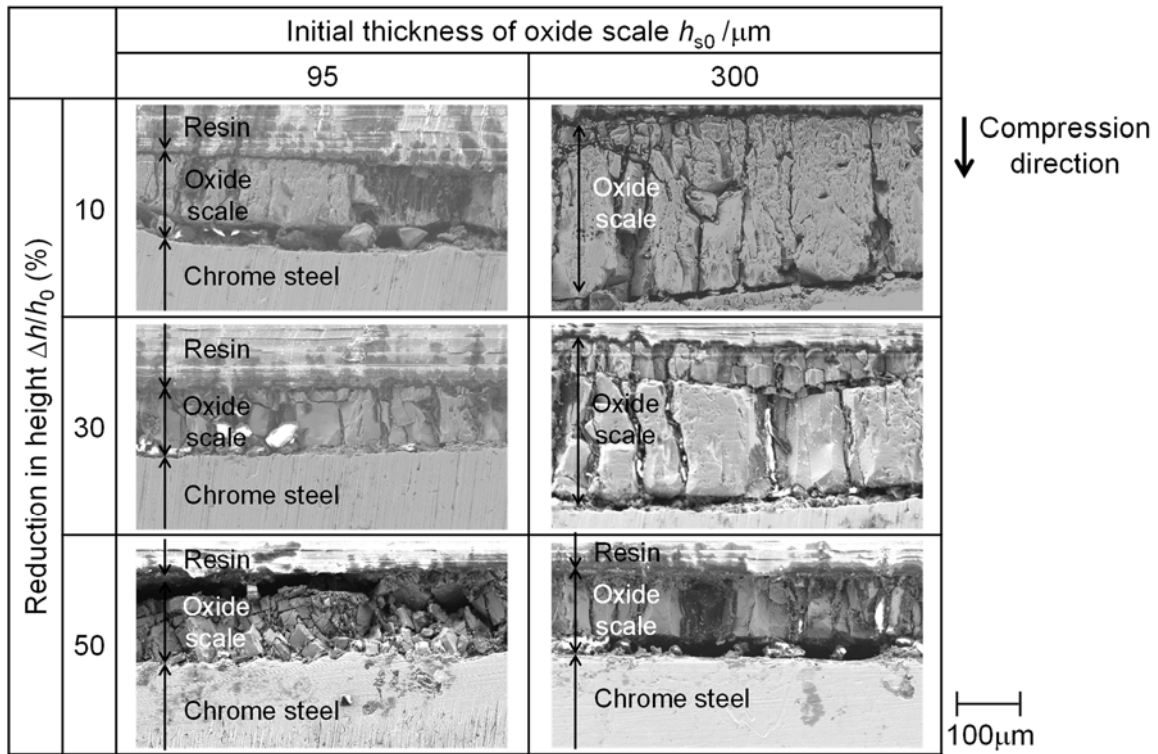


Fig. 11 SEM photographs of cross-section of oxide scale–chrome steel workpiece interface after the ring compression test.

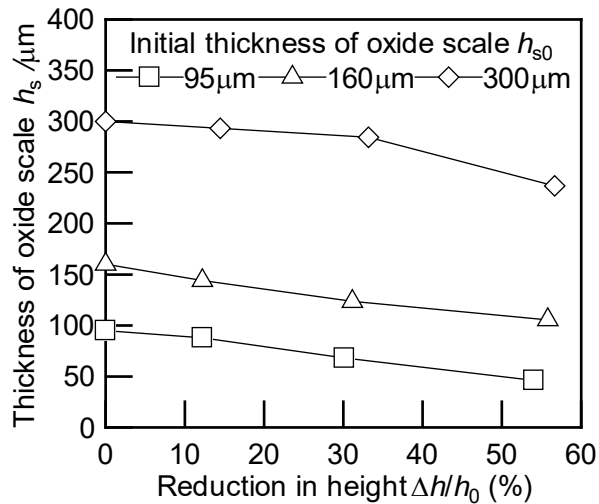


Fig. 12 Thickness of oxide scale on a chrome steel surface after the ring compression test.

## 5. Finite element analysis results

The friction at the tool–scale contact was estimated from the relationship between the

coefficient of shear friction at the tool–scale contact ( $m_{t-s}$ ) and the plastic deformation of the workpiece prepared with a scale layer was based on the finite element simulation calculation. In the calculation, the friction of the tool–workpiece contact was assumed to be constant,  $m_{t-w} = 0.80$ , based on the results of the ring compression test for a workpiece having a thin scale film with  $h_{s0} = 6 \mu\text{m}$  (Fig. 8). Figure 13 shows the calculated results of the change in the inner diameter of the workpiece having a scale film with  $h_{s0} = 300 \mu\text{m}$ . The experimental results of the ring compression test for a workpiece having a scale film with  $h_{s0} = 300 \mu\text{m}$  are also plotted in Fig. 13. The nominal coefficient of shear friction at the tool–scale contact was determined to be  $m_{t-s} = 0.40$ , based on a comparison between the calculated (line) and experimental (mark) results presented in Fig. 13. The estimated friction at the tool–scale contact ( $m_{t-s} = 0.40$ ) was lower than the friction at the tool–workpiece contact ( $m_{t-w} = 0.80$ ).

Figure 14 shows the calculated and experimental results of the changes in the inner diameter of the workpiece covered with a scale layer after conducting the ring compression test, for friction coefficients for the tool–workpiece and tool–scale contacts of  $m_{t-w} = 0.80$  and  $m_{t-s} = 0.40$ , respectively. Thicker initial scale layers provided higher changes in the calculated inner diameter ( $d/d_0$ ). The nominal coefficient of a workpiece covered with a scale layer was calculated based on the results presented in Fig. 14 using the calibration curves for the relationship between the coefficient of shear friction and the change in the inner diameter. The obtained nominal coefficient of shear friction for the tool–workpiece covered with a scale layer is shown in Fig. 15. Thicker initial thickness of the scale layers provided lower nominal coefficients of shear friction. The calculated and experimental results agreed well, however, the calculated coefficient of shear friction did not change significantly with the scale thickness. Several mechanisms could explain the observed results. (1) Although the obtained coefficients of shear friction were not constant, as shown in Fig. 8, the coefficients of shear friction associated with the tool–workpiece and tool–scale contacts were constant in the calculation.

(2) The scale was not allocated to the inner and outer peripheries of the workpiece in the finite element model. After the middle stage of the ring compression process, the scale located initially on the surfaces of the inner and outer peripheries of the workpiece contacted the tools in the experiment. (3) The heat transfer coefficients at each boundary of the tool, workpiece, and scale layer were assumed to be constant (no considerations of temperature and contact pressure dependencies).

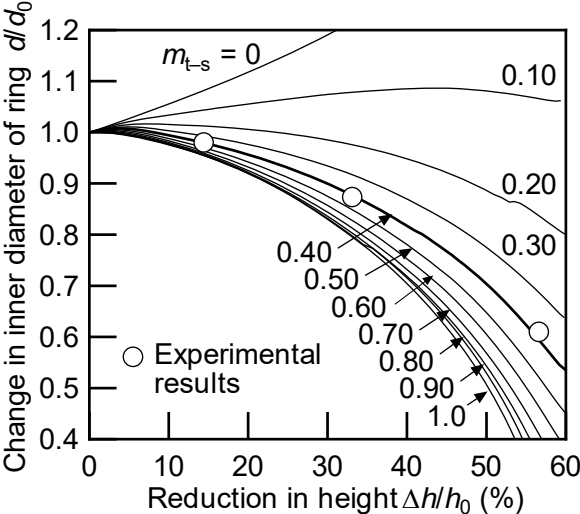


Fig. 13 Influence of coefficient of shear friction of tool–oxide scale contact ( $m_{t-s}$ ) on change in inner diameter of the chrome steel workpiece covered with oxide scale layer in the ring compression test ( $m_{t-w} = 0.80$ ,  $h_{s0} = 300 \mu\text{m}$ ).

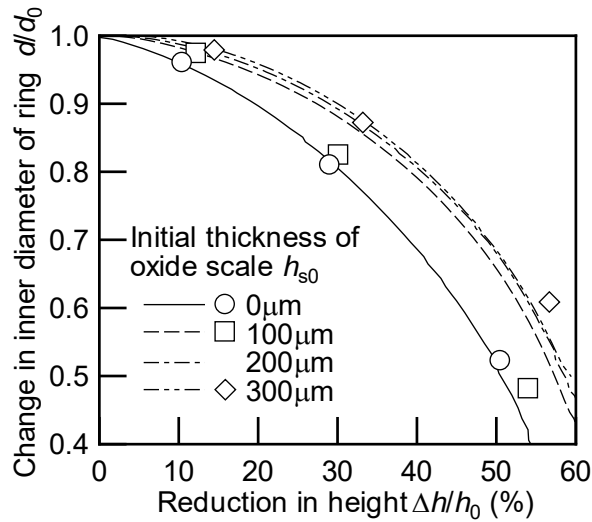


Fig. 14 Change in inner diameter of the chrome steel workpiece covered with oxide scale layer in the ring compression test ( $m_{t-w} = 0.80$ ,  $m_{t-s} = 0.40$ ) (line: FEM, mark: experiment).

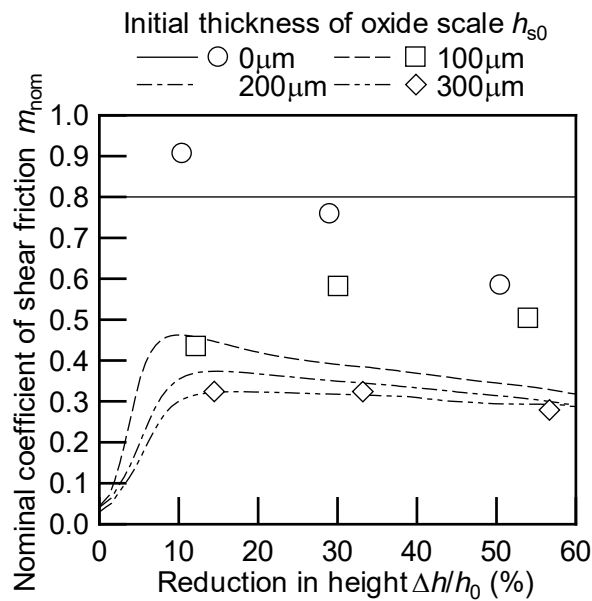


Fig. 15 Nominal coefficient of shear friction of the chrome steel workpiece covered with oxide scale layer in the ring compression test ( $m_{t-w} = 0.80$ ,  $m_{t-s} = 0.40$ ) (line: FEM, mark: experiment).

## 6. Discussions on the mechanism of underlying the friction reduction

The mechanism by which the scale film reduced the friction at the workpiece surface

was examined based on the finite element analysis from the perspective of the thermal and frictional characteristics of the scale. Figure 16 shows the calculated temperature distribution of the workpiece covered with a scale layer during the ring compression test. The initial temperature of the workpiece covered with a scale layer was uniformly  $T_0 = 1273$  K. The temperature of the workpiece covered with a scale layer changed during the ring compression test due to the heat generation by the plastic deformation and the heat transfer between the workpiece, scale layer and tool. The workpiece covered with a scale layer remained at a high temperature during compression, whereas the temperature of the workpiece without scale layer dropped sharply during compression. Because the thermal conductivity of FeO (the primary composition of the scale) is lower than that of the chrome steel (Touloukian et al., 1970; Akiyama et al., 1991), the scale reduced the heat transfer rate at the workpiece–tool contact interface. The calculated temperature changes in the workpiece at the center and the scale–workpiece interface parts during the ring compression test are shown in Fig. 17. Regardless of the scale thickness, the temperatures at the center part of the workpiece remained the same. Thicker initial scale layer provided higher calculated temperature at the scale–workpiece interface part. The low conductivity of the scale reduced the forging load of the workpiece covered with a scale layer relative to the forging load on the workpiece without scale layer, as shown in Fig. 9.

The influence of low thermal conductivity of the scale on the plastic deformation of the workpiece covered with a scale film was examined. Figure 18 shows the calculated nominal coefficient of shear friction at the tool–workpiece contact during the ring compression test. The nominal coefficient of shear friction for the workpiece covered with a scale layer was calculated based on the observed change in the inner diameter of the workpiece using the calibration curves describing the relationship between the coefficient of shear friction and the change in the inner diameter. For the case of identical coefficients of

shear friction at the tool–workpiece ( $m_{t-w}$ ) and tool–scale layer ( $m_{t-s}$ ) contacts ( $m_{t-w} = m_{t-s} = 0.80$ ), the nominal coefficients for the workpieces having scale layers with  $h_{s0} = 100$  and  $300 \mu\text{m}$  were lower than the coefficient for a workpiece without scale layer ( $m_{\text{nom}} = 0.80$ ). This result indicated that the nominal coefficient of shear friction was reduced only due to the low thermal conductivity of the scale. The shear friction values for the workpieces having scale layers with  $h_{s0} = 100$  and  $300 \mu\text{m}$  were further reduced, according to the calculations ( $m_{t-w} = 0.80$  and  $m_{t-s} = 0.40$ ). The calculated nominal coefficients of shear friction for the workpiece without scale layer ( $m_{t-w} = 0.80$ ) and with a scale layer ( $m_{t-w} = m_{t-s} = 0.80$ ) differed only due to the low thermal conductivity of the scale. The calculated nominal coefficients of shear friction for the case in which  $m_{t-w} = m_{t-s} = 0.80$  and the case in which  $m_{t-w} = 0.80$ ,  $m_{t-s} = 0.40$  differed due to low friction characteristics of the scale.

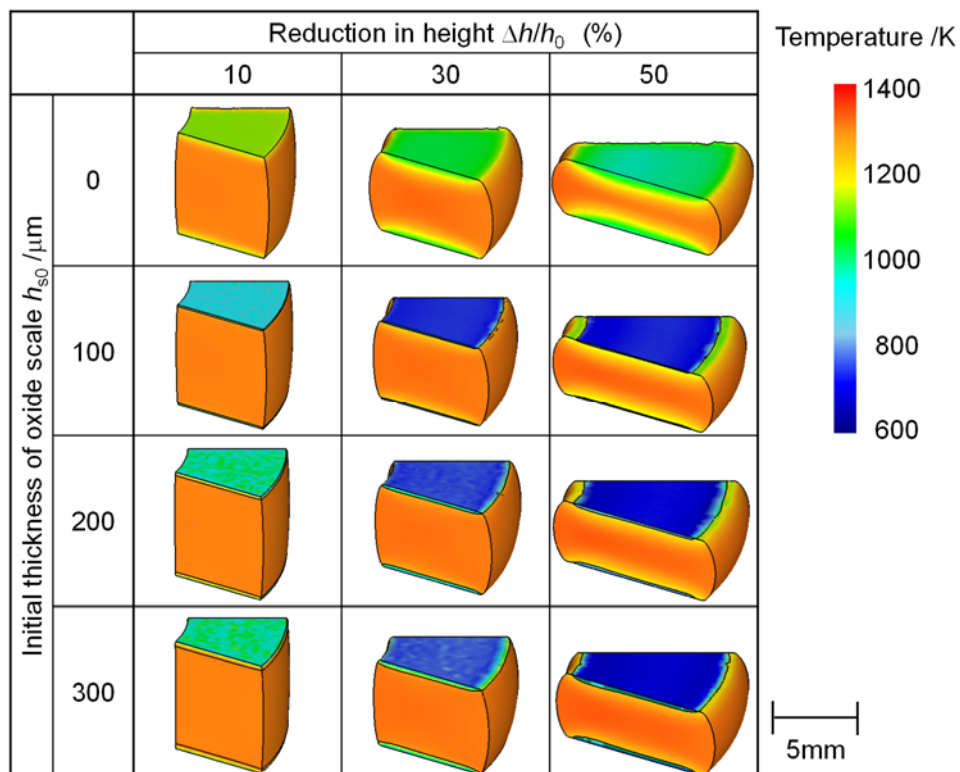
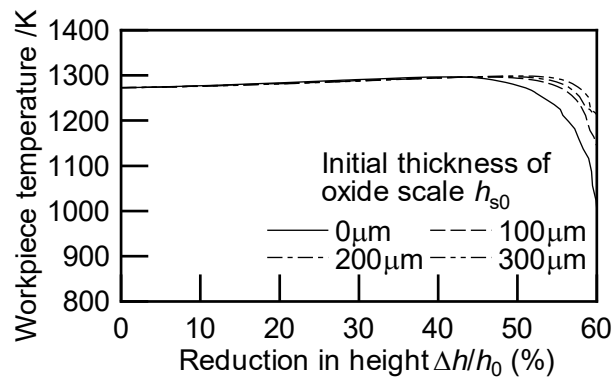
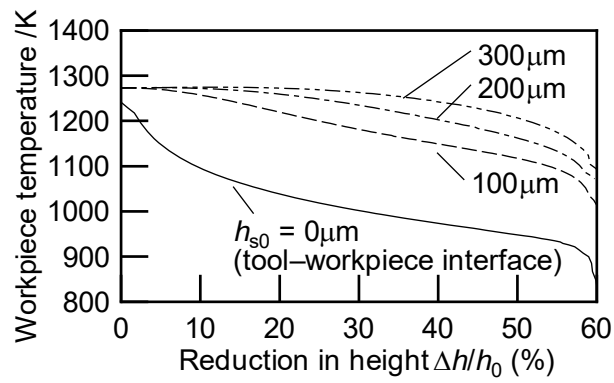


Fig. 16 Calculated temperature distribution in the chrome steel workpiece covered with oxide scale layer during the ring compression test ( $m_{t-w} = 0.80$ ,  $m_{t-s} = 0.40$ ).



(a) Center part of chrome steel workpiece.



(b) Interface part of oxide scale-chrome steel workpiece.

Fig. 17 Calculated temperature changes in the chrome steel workpiece covered with oxide scale layer during the ring compression test ( $m_{t-w} = 0.80$ ,  $m_{t-s} = 0.40$ ).

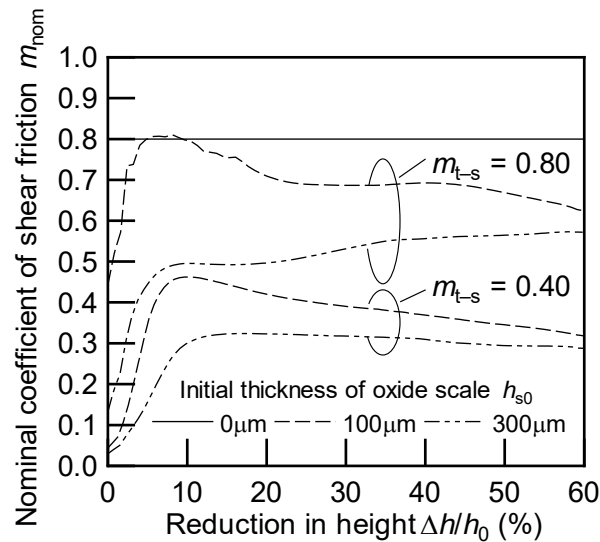


Fig. 18 Nominal coefficient of shear friction for the chrome steel workpiece covered with oxide scale layer during the ring compression test ( $m_{t-w} = 0.80$ ).

## 7. Conclusions

The hot ring compression test of chrome steel covered with an oxide scale film was carried out to examine the effects of the oxide scale film on the hot forging characteristics. The effects were investigated both experimentally and using finite element analysis calculations. In the finite element analysis, the plastic deformation and temperature changes of the steel workpiece and the oxide scale layer were calculated to discuss the mechanism by which the friction was reduced during hot forging process. The following conclusions were obtained.

- (1) The oxide scale maintained a high temperature in the steel workpiece during hot forging due to the low thermal conductivity of the oxide scale. Owing to this character, the forging load of the workpiece covered with an oxide scale film is reduced.
- (2) The oxide scale displayed low friction characteristics during hot forging in this study. The oxide scale may potentially act as a lubricant during hot forging processes under specific forging conditions.

## Acknowledgement

This work was financially supported in part by the Research Committee for Oxide Scale Behavior in Steel Manufacturing Processes, Iron and Steel Institute of Japan.

## References

- Abuluwefa, H.T., Guthrie, R.I.L., Ajersch, F., 1997, Oxidation of low carbon steel in multicomponent gases: Part II Reaction mechanisms during reheating. *Metallurgical and Materials Transactions A*. 28(8), 1643-1651.
- Akiyama, T., Ogura, G., Ohota, H., Takahashi, R., Waseda, Y., Yagi, J., 1991, Thermal conductivities of dense iron oxides. *Tetsu-to-Hagané*. 77(2), 231-235.
- Behrens, B.-A., Doege, E., Reinsch, S., Telkamp, K., Daehndel, H., Specker, A., 2007, Precision forging processes for high-duty automotive components. *Journal of Materials Processing Technology*. 185(1-3), 139-146.
- Callister, W.D., 2006, *Materials science and engineering: An introduction*, 7th edition. John Wiley & Sons, Inc., New York, 320-322.
- Doege, E., Bohnsack, R., 2000, Closed die technologies for hot forging. *Journal of Materials Processing Technology*. 98(2), 165-170.
- Douglas, R., Kuhlmann, D., 2000, Guidelines for precision hot forging with applications. *Journal of Materials Processing Technology*. 98(2), 182-188.
- Garza-Montes-de-Oca, N.F., Rainforth, W.M., 2009, Wear mechanisms experienced by a work roll grade high speed steel under different environmental conditions. *Wear*. 267(1-4), 441-448.
- Gladkov, Y., 2006, Hot-die forging press with adaptive CNC for hot-die precision forging. *Proceedings of the JSTP International Seminar on Precision Forging*. 105-110.
- Graf, M., Kawalla, R., 2011, Deformation behaviour and mechanical properties of oxide

- scales during hot metal forming processes. *Steel Research International*. 82, Special Edition, ICTP 2011, 78-81.
- Graf, M., Kawalla, R., 2012, Characterization of multilayered oxide scale. *Steel Research International*. Special Edition, 979-982.
  - Guerrero, M.P., Flores, C.R., Pérez, A., Colás, R., 1999, Modelling heat transfer in hot rolling work rolls. *Journal of Materials Processing Technology*. 94(1), 52-59.
  - Hara, K., Utsunomiya, H., Sakai, T., Yanagi, S., 2011, Influence of oxide scale on hot rolling characteristics of steel sheets. *Steel Research International*. 82, Special Edition, ICTP 2011, 74-77.
  - Hidaka, Y., Anraku, T., Otsuka, N., 2002, Tensile deformation of iron oxides at 600-1250°C. *Oxidation of Metals*. 58(5/6), 469-485.
  - Kada, O., Miki, T., Toda, M., Osakada, K., 1998, Calculation of isothermal flow stress by combination of FEM and simple compression test. *CIRP Annals – Manufacturing Technology*. 47(1), 185-188.
  - Krzyzanowski, M., Beynon, J.H., 2002, Measurement of oxide properties for numerical evaluation of their failure under hot rolling conditions. *Journal of Materials Processing Technology*. 125-126(9), 398-404.
  - Krzyzanowski, M., Beynon, J.H., Farrugia, D.C.J., 2010, Oxide scale behavior in high temperature metal processing. Wiley-VCH Verlag GmbH & Co. KGaA, Weinheim, 80-89.
  - Male, A.T., Cockcroft, M.G., 1964-65, A method for the determination of the coefficient of friction of metals under conditions of bulk plastic deformation. *Journal of the Institute of Metals*. 93, 38-46.
  - Munther, P.A., Lenard, J.G., 1999, The effect of scaling on interfacial friction in hot rolling of steels. *Journal of Materials Processing Technology*. 88(1-3), 105-113.

- Nakasaki, M., Myochin, H., Nakamizo, T., Takasu, I., 2006, Process improvements of hot forging with hub bearing parts by applying 3-D CAE analysis. Proceedings of the JSTP International Seminar on Precision Forging. 111-116.
- Okada, H., 2003, Deformation of scale in hot strip rolling. Journal of the Japan Society for Technology of Plasticity. 44(505), 94-99. (in Japanese)
- Schey, J.A., 1983, Tribology in metalworking: Friction, lubrication, and wear (ASM International). American Society for Metals, Metals Park.
- Stanley, J.K., Hoene, J. von, Huntoon, R.T., 1951, The oxidation of pure iron. Transactions of American Society for Metals. 43, 426-446.
- Suárez, L., Rodríguez-Calvillo, P., Houbaert, Y., 2011, Analysis of deformed oxide layers grown on steel. Oxidation of Metals. 75(5-6), 281-295.
- Torres, M., Colás, R., 2000, A model for heat conduction through the oxide layer of steel during hot rolling. Journal of Materials Processing Technology. 105(3), 258-263.
- Touloukian, Y.S., Buyco, E.H., 1970, Specific heat – metallic elements and alloys, Thermophysical Properties of Matter. Volume 4, 687-689.
- Touloukian, Y.S., Powell, R.W., Ho, C.Y., Klemens, P.G., 1970, Thermal conductivity – metallic elements and alloys. Thermophysical Properties of Matter. Volume 1, 1152-1159.
- Utsunomiya, H., Doi, S., Hara, K., Sakai, T., Yanagi, S., 2009, Deformation of oxide scale on steel surface during hot rolling. CIRP Annals – Manufacturing Technology. 58(1), 271-274.